ChemistryOPEN Full Papers

ChemPubSoc Europe

Open Access

DOI: 10.1002/open.201402009

Gold Nanowire Forests for SERS Detection**

Andrea La Porta,[a] Marek Grzelczak,[a, b] and Luis M. Liz-Marzán*[a, b]

Simple wet chemistry has been applied to control the vertical growth of gold nanowires on a glass substrate. As a consequence, the longitudinal localized surface plasmon band position can be tuned from 656 to 1477 nm in a few minutes by simply controlling the growth rate and time. This allowed us to select the optimum conditions for maximum electromagnetic enhancement and performance in surface enhanced Raman scattering (SERS) detection. SERS measurements confirmed the uniform and reproducible distribution of the nanowires on the substrate, with the subsequent high reproducibility of hot spot formation. Detection of malachite green in water and of 1-naphthalenethiol from the gas phase are demonstrated as proof-of-concept applications of these three-dimensional SERS substrates.

Introduction

Surface-enhanced Raman scattering (SERS) is a powerful analytical tool, mainly based on the interaction of the high electromagnetic fields generated at the surface of metal nanostructures when illuminated at their corresponding localized surface plasmon resonances (LSPRs). Such enhanced near fields are typically favored at small gaps between nanoparticles that are known as hot spots.[1–3] Recent progress in metal processing techniques and in colloid chemistry methods has driven a large amount of research focusing on the fabrication of high-performance SERS substrates and their application in various fields.[4–12] Nanoparticles (NPs) with a wide variety of shapes have been used to create substrates with a high density of hot-spots, reaching enhancements of the Raman signal by many orders of magnitude.[13–19] The main challenge regarding the fabrication of SERS substrates however concerns their uniformity and reproducibility. One of the most studied methods to create hot spots is the self-assembly of metallic NPs (bottom-up approach), and many efforts are being spent to reach a suitable control over this technique. Recent examples include the self-assembly of Au[20] and Au@Ag[15] nanorods into supracrystals, which have been applied to the detection of scrambled prions and other bio-relevant molecules. In a related report, Zhu et al.[21] demonstrated the detection of microcystin LR (MC-LR), a toxin produced by an algae, exploiting the electric field enhancement occurring at the hot spots of an end-to-end assembly of Au nanorods. In particular, they detected the SERS signal of the probe molecule 4-aminothiophenol (4-ATP), which is highly dependent on the MC-LR concentration in solution. Zheng et al.[22] used DNA-directed self-assembly of spherical particles of different sizes to create a core-satellite plasmonic structure and fabricate a reproducible SERS substrate. By changing the Au NP concentration and the number of DNA chains per NP, they were able to control the distance between each core Au NP and, as a consequence, the optical properties of the substrate. SERS experiments showed a limit of detection of 10^{-9} M for benzenethiol.

Alternatively, top-down methods, including focused ion beam (FIB) and electron beam lithography (EBL), have been used to deposit nanostructures on solid substrates with high precision, thereby controlling the NPs size and shape, as well as interparticle distance.[23–28] These fabrication methods opened new possibilities to realize highly ordered and reproducible SERS supports. Examples include the work by Wells et al.,[29] who fabricated "isolated" nanopillars by using a combination of EBL, metal mask lift-off patterning and reactive ion etching. SERS measurements of a thin layer of zinc phthalocyanine showed that the SERS enhancement largely depends on the physical features of the nanopillars, such as height, diameter and shape. Nanopillars have also been fabricated by Boisen et al.[30] by using a maskless approach. In this work they exploit the bending capability of standing nanopillars to create hot spots and achieve picomolar SERS detection. However, next to these advantages top-down approaches also present certain drawbacks such as the need for very sophisticated equipment and high cost. This represents a significant limitation in the large-scale fabrication of substrates, which may be overcome by improving the control over the relatively inexpensive self-assembly approaches.

In this paper, we present a simple and highly reproducible procedure to control the optical response of gold nanowires (Au NWs), vertically grown on top of a silanized glass support.

[a] A. La Porta, Dr. M. Grzelczak, Prof. L. M. Liz-Marzán
Bionanoplasmonics Laboratory, CIC biomaGUNE
Paseo de Miramón 182, 20009 Donostia-San Sebastián (Spain)
E-mail: llizmarzan@cicbiomagune.es

[b] Dr. M. Grzelczak, Prof. L. M. Liz-Marzán
Ikerbasque, Basque Foundation for Science
48011 Bilbao (Spain)

[**] This article is part of the Virtual Special Issue "Molecular Sensors"

Supporting information for this article is available on the WWW under http://dx.doi.org/10.1002/open.201402009.

A high control over the LSPR of the NWs was achieved by tuning growth time, which allowed us to tailor the resonance wavelength of the collective Au NW plasmon band with good accuracy, within the near infrared (NIR) region. The growth of Au NWs is demonstrated to be homogeneous over the whole glass surface, and to provide a large enhancement of the SERS signals of mercaptobenzoic acid (MBA), used during the synthesis. Removal of MBA from the Au NWs resulted in highly efficient SERS substrates for the detection of malachite green (MG), a carcinogenic and antibacterial compound.[31–34] Plasma cleaning allowed us to recycle the substrates, and we also demonstrate the possibility to detect molecules from the gas phase by using 1-naphthalenethiol (1-NAT) as a volatile probe.

Results and Discussion

The growth of vertical Au NWs on glass substrates was based on the method recently reported by He et al.[35] This method comprises three steps: glass functionalization with an aminosilane (3-aminopropyltriethoxy silane, APTES), seed self-assembly and seeded growth. The key element behind the preferential anisotropic growth perpendicular to the substrate seems to be the use of MBA to functionalize the Au NP seeds upper surface, which is not possible on the lower part because of the presence of APTES binding the NP to the glass surface. This results in the reduction of Au^{III} only at the bottom side of the seeds, which acts as catalysts. As a consequence, each seed is lifted up from the glass, and the reduced gold atoms are covered by MBA molecules present in solution, thereby forcing the reduction to occur always at the bottom side. Whereas the diameter of the NWs depends on the ratio between MBA and Au^{III} in solution, their length can be readily controlled through the growth time. The resulting increase in the aspect ratio was readily observed through changes in the Vis/NIR spectra (Figure 1 A). As the NWs grow longer, redshift and broadening are observed in the plasmon band, with a new band developing after 4–5 min. After 10 min of NW growth, two distinct bands can be discerned, one centered around 600 nm and a broader one around 1500 nm. Although the bands become very broad after Au NW growth, this process proved to be highly reproducible, as shown in Figure 1 B, where the maximum positions of the low-energy bands are plotted versus growth time for three different synthesis series, each comprising seven substrates that were grown for different times. The LSPR spectra in Figure 1 A are the result of plasmon coupling between individual NWs. Interestingly, the LSPR of (non-coupled) NWs in solution (not shown) shows a red-shifted longitudinal band, which is in agreement with the results by Funston et al.[36] for side-by-side aligned nanorods. The NW substrate used in our work can be considered as many side-by-side aligned NWs, so that by changing the growth time, it is possible to control not only the LSPR of the individual NWs but also their collective coupling behavior. It is important to highlight that the growth solution used for the synthesis always consisted of freshly prepared MBA and ascorbic acid stock solutions, meaning that changes arising from potential errors in this preliminary step do not appear to affect NW growth. From Figure 1 A it is however not perfectly clear at which point of the synthesis the nanowire shape starts to develop. Indeed, for growth times up to 3 min a single plasmon band is visible in the spectrum. Transmission electron microscopy (TEM) was used to analyze the formed particles, upon detachment from the substrate (see Experimental Section for details). The electron micrographs show that already after one minute of growth, anisotropic nanoparticles are formed but with rather undefined shapes (Figure S1, Supporting Information). After 2 min, the aspect ratio has increased and a rod-like morphology is clearly observed; whereas after 3 min, NWs have definitely been formed. Systematic experiments (data not shown) evidenced that the growth rate can be controlled by varying the amounts of Au^{III} and MBA in the growth solution while keeping a constant molar ratio between them. Another important factor influencing the overall growth rate is the number of seeds acting as catalysts: at fixed [Au^{III}]/[MBA] ratio, increasing the seed density on the substrate leads to slower NW growth because of a lower amount of Au^{III} per seed. This is an important issue in terms of reproducibility in NW length. Figures 1 C–E show scanning electron microscopy (SEM) images of three substrates grown for 3, 7 and 10 min, displaying the resulting density of NWs on the glass substrate as well as their tendency to bend and form bundles. Details about the dimensions were obtained from TEM images as shown in Figures 1 F–H. The average diameter does not vary during growth and is determined by the MBA/Au^{III} molar ratio in the growth solution (0.48 in these sam-

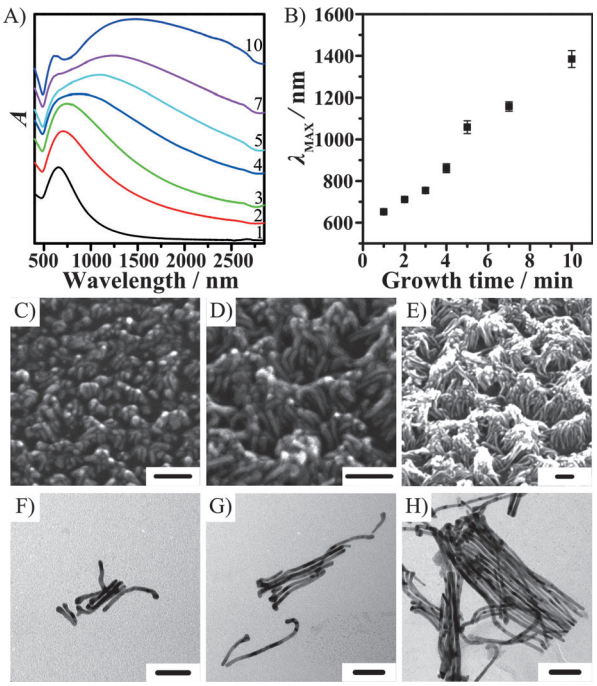

Figure 1. A) Absorbance spectra of Au NWs for different growth times as labeled (min). B) Wavelength of the maximum of the lower energy plasmon band, as a function of growth time. Each point is the result of an average over three different substrates, and the error bar indicates high synthesis reproducibility. C–E) SEM images of Au NWs on glass after 3 (C), 7 (D) and 10 min (E). F–H) Corresponding TEM images of Au NWs from the same substrates. All scale bars represent 50 nm.

ples), and it was determined to be 5.34±0.76 nm. A statistical analysis reveals that after 3, 7 and 10 min the NW lengths are 68±9, 198±26 and 334±47 nm, respectively.

The SERS efficiency and reproducibility of the substrates was evaluated by preparing three different series of samples and measuring the MBA SERS signal corresponding to the ν(C–C) mode[37] at 1075 cm^{-1} for each of them (Figure S2A, Supporting Information). The observed trend was the same for all series, and the maximum SERS intensity was always recorded for the substrates that were grown for 4 min, though almost no difference was observed when comparing 3, 4 and 5 min growth. The plasmon band for these substrates was centered around 740 nm, which is in close resonance with the laser wavelength used for SERS excitation (785 nm). Therefore, we decided to use these growth conditions in all subsequent experiments. The high uniformity of the samples was demonstrated by recording MBA SERS spectra at 30 different spots covering the whole area of the same substrate (1 cm^2) and performing a statistical analysis of the results (Figure S2B, Supporting Information). Remarkably, almost all the points fell into the light-blue area, which represents a fluctuation of ±5% from the mean value. To optimize the performance of a SERS substrate, it is important to fully exploit the enhanced near field, which is created in close proximity to the NWs surface.[38] To facilitate access of the analytes to the NWs surface, we used Ar^+ plasma cleaning to remove the MBA organic layer covering the NWs, which plays a key role during the synthesis process. As shown in Figure 2A, after Ar^+ plasma cleaning, no significant changes were observed in the UV/Vis spectrum, while the efficiency in removing MBA from the surface was confirmed by measuring the MBA SERS signal before and after cleaning (Figure 2B): all the SERS peaks disappeared, meaning that the resulting NW surface was free of MBA molecules. SEM analysis after Ar^+ plasma treatment revealed that the NWs were only slightly modified by the plasma while keeping their morphology and 3D organization (Figure S3, Supporting Information). The resulting MBA-free NWs were tested as a SERS sensor for the detection of malachite green (MG). MG is an organic dye, which has an effective fungicide effect that is widely used in fish farms, in the aquaculture industry and in freshwater aquaria. However, the use of malachite green is rather controversial due to its genotoxic and carcinogenic nature, and it is banned in several countries.[39] Figure 2C shows the recorded MG SERS spectra after dipping the sample in aqueous solutions containing different concentrations of MG, down to 10^{-6} M. By plotting the average intensity of the C–C stretching peak at 1618 cm^{-1} as a function of MG concentration (Figure 2D), we find that the peak intensity reaches a plateau around 0.5 mM MG, which is an evidence behind complete NW coverage by MG molecules.

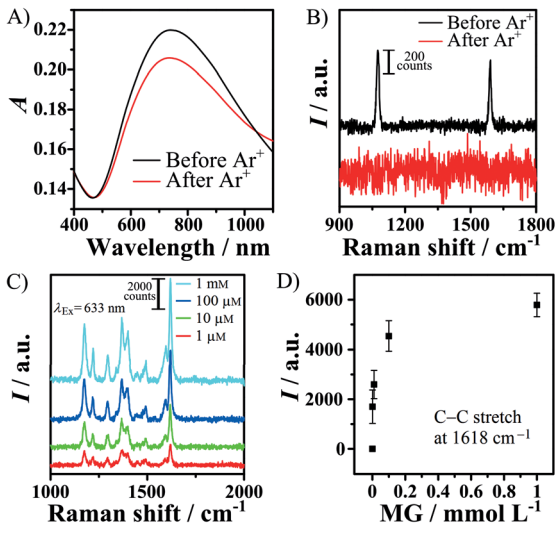

Figure 2. A,B) UV/Vis and SERS spectra of an Au NW substrate before and after Ar^+ plasma cleaning: no significant changes are observed while complete removal of MBA from the Au surface is confirmed by the loss of MBA SERS signal. C) SERS spectra of MG at different molar concentrations: the characteristic MG peaks are clearly visible down to 10^{-6} M. D) Intensity of the C–C stretching peak versus MG concentration. Data in C and D are averages from three measurements.

Since plasma cleaning has been shown to remove adsorbed molecules from the Au NWs with no significant alteration of their morphology and optical response, we tested reusability of the substrates for detection of different analytes. Thus, after MG sensing, the same substrate was used to detect 1-naphthalenethiol (1-NAT) and rhodamine 6G (R6G), and the results are shown in Figure 3. MBA was first removed (Figure 3A) and MG was adsorbed and detected by SERS (Figure 3B). A second Ar^+ plasma cleaning treatment was then applied to remove MG, and 1-NAT was allowed to absorb onto the Au NW surface (Figure 3C). Finally, a third plasma cleaning step enabled the detection of R6G (Figure 3D). In each SERS spectrum, all the main features of the corresponding analyte were visible: ν(C–C) and ring breathing at 1075 and 1589 cm^{-1}, respectively, for MBA,[37] δ(C–H) and ν(N-Φ) for MG,[40] δ(C–H) and ring stretch for 1-NAT,[41] ν(C–C) and ν(C–N) for R6G.[42] Complete band assignment is provided in Table S1 (Supporting Information). The corresponding UV/Vis spectra at each step revealed some broadening after the first plasma cleaning process, but no significant variations until the end of the entire cycle (Figure S4, Supporting Information).

Further application of the substrates was found for detection from the gas phase, using 1-NAT as Raman probe. The simple experimental setup is shown in Figure 4A. A 25 mL plastic tube was used as a chamber in which the substrate was fixed to the inner side of the cap, while single drops (25 μL) of 1-NAT solutions in ethanol at selected concentrations were deposited on the bottom of different tubes. The SERS spectra in Figure 4B confirm the detection of the volatile 1-NAT, down to a concentration of 10^{-3} M in the liquid drop. The adsorption of 1-NAT on the Au NW forest could be monitored by registering the SERS peak intensity at 1559 cm^{-1}, as a function of time. As expected, the SERS intensity increased with time (Figure 4C), indicating the gradual evaporation of 1-NAT from the drop until the Au NW surface was saturated. It is important to note that 10^{-3} M is the concentration of 1-NAT in the liquid, so the maximum concentration of 1-NAT in the 25 mL tube volume would be 10^{-6} M, assuming that all the molecules in the drop are evaporated. Additionally, part of the molecules are expect-

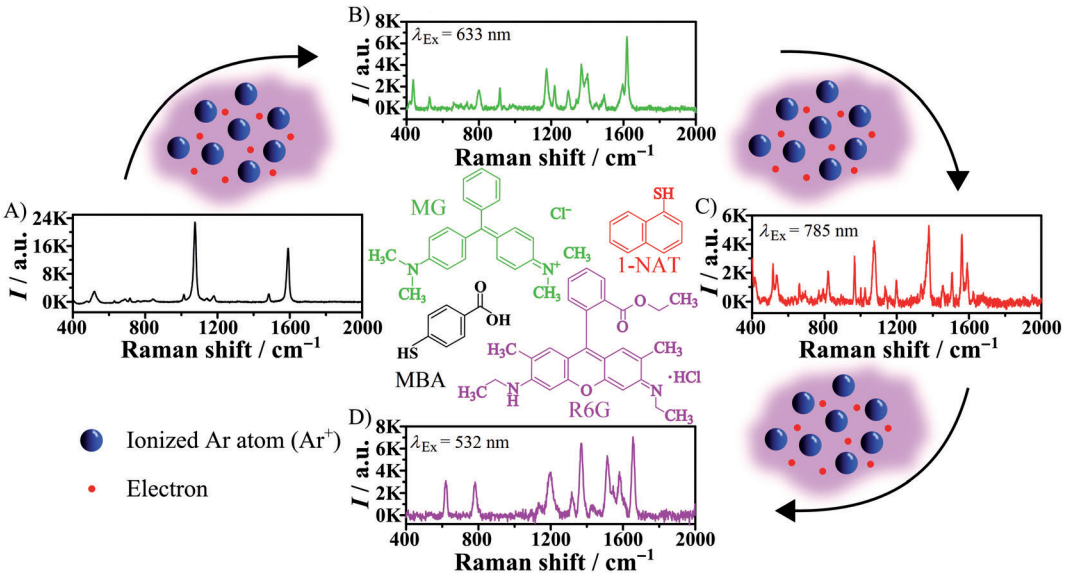

Figure 3. Illustration of a detection cycle of MG, 1-NAT and R6G upon removal of MBA molecules from the Au NWs substrate. A) SERS spectrum of MBA right after the synthesis. B–D) SERS spectra of MG (B), 1-NAT (C) and R6G (D) after successive Ar^+ plasma cleaning and dipping the substrate in the corresponding solution. Dipping time was 1 h for all samples.

ed to adsorb onto the tube walls, not contributing to the internal pressure. At this upper limit of 1-NAT concentration, saturation of the SERS signal was reached after 50 min.

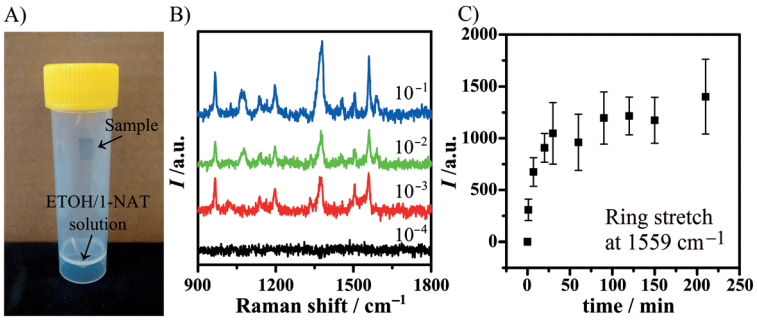

Figure 4. A) Illustration of the experimental setup for gas phase detection: after Ar^+ cleaning the substrate was attached to the cap of a 25 mL tube containing an EtOH/1-NAT solution (25 μL). B) SERS spectra measured for different 1-NAT concentrations inside the tube: typical features of 1-NAT spectrum are distinguishable down to 10^{-3} M. C) Intensity of the ring stretching peak at 1559 cm^{-1} versus time: saturation was reached at around 50 min incubation time.

Conclusions

We have demonstrated a simple and highly reproducible method for the vertical growth of densely packed gold nanowires (Au NWs) on 3-aminopropyltriethoxy silane (APTES)-functionalized glass slides, which allows fine tuning of the LSPR response in the NIR. This optical control allowed us to tune the plasmon band in the proximity of the excitation laser wavelength used for SERS measurements, thereby achieving high electric field enhancements at the surface of the NWs. Mercaptobenzoic acid (MBA) can be completely removed from the substrates by plasma cleaning without damage of the nanostructure, allowing its use as a sensor, which was demonstrated through the detection of malachite green (MG) in aqueous solution with a limit of detection of 10^{-6} M. We also demonstrated the reusability of the sensor by successive plasma cleaning after detection of each analyte. We were thus able to detect MG, 1-naphthalenethiol (1-NAT) and rhodamine 6G (R6G) by recycling the same substrate. As a final application of this system, gas sensing efficiency was demonstrated by detecting 1-NAT evaporated from solution. Thus, this is a robust and highly versatile system that can be implemented for multiple detection uses. The detection efficiency might however be improved by using an infrared laser source which couples to longer Au NWs.

Experimental Section

Chemicals: 3-Aminopropyl triethoxysilane (APTES, ≥98%), sodium borohydride ($NaBH_4$, 99%), gold(III) chloride trihydrate ($HAuCl_4$, ≥99.9%), 4-mercaptobenzoic acid (MBA, 90%), L-ascorbic acid (≥99%), sodium citrate tribasic dihydrate (≥98%), malachite green chloride (≥96%), 1-naphthalenethiol (99%), and rhodamine 6G (95%) were purchased from Sigma–Aldrich. Hydrogen peroxide (H_2O_2, 35% *w/w*) and sulphuric acid (H_2SO_4, 96%) were purchased from Scharlau and Panreac, respectively. Glass slides (24×24 mm^2) were purchased from Menzel-Gläser.

Characterization: Optical extinction spectra were recorded using an Agilent 8453 UV/Vis diode-array spectrophotometer. UV/Vis/NIR spectra were collected using a scanning spectrophotometer Varian, Cary5000. The samples were treated with Ar^+ plasma using AJA-ATC 1800 UHV Magnetron Sputtering. SERS spectra were recorded using a Renishaw Invia Raman microscope equipped with two Pelt-

ier-cooled CCD detectors, a Leica microscope two gratings with 1200 and 1800 lines/mm and band-pass filter optics. Excitation lasers with emission wavelengths of 785, 633 and 532 nm were used and focused onto the sample through a 100× objective with N.A. 0.85, this producing a spot size of 923, 745 and 626 nm^2 for 785, 633 and 532 nm, respectively. The SERS spectra were collected with an integration time of 10 s, and the samples were irradiated with constant powers of 1.2 mW (785 nm), 0.05 mW (633 nm) and 0.1 mW (532 nm). Transmission electron microscopy (TEM) images were collected with a JEOL JEM-1400PLUS instrument operating at 120 kV. Scanning electron microscopy (SEM) was measured with a dual beam FIB - FEI Helios 450S microscope with electron column resolution of 0.8 nm at 20 kV.

Synthesis of Au seeds: An aqueous solution (20 mL) containing $HAuCl_4$ (1.25×10^{-4} M) and sodium citrate (2.5×10^{-4} M) was heated to 50 °C, and a freshly prepared $NaBH_4$ solution (300 μL, 10^{-2} M) was added under vigorous stirring. After 30 s, stirring was slowed down and maintained for 15 min. The UV/Vis spectrum of the solution showed an absorbance band at 509 nm.

Preparation of the substrates: Each glass slide was first treated with piranha solution (H_2SO_4/H_2O_2 3:1) for 60 min, then rinsed with abundant distilled H_2O and dried under with N_2. The substrates were then immersed in an APTES/EtOH solution (5% *v/v*) overnight. After washing with EtOH to remove excess APTES and drying under N_2, they were soaked in the seed solution for 60 min, followed by rinsing with distilled H_2O and drying under N_2.

Au NW synthesis: The seed-functionalized part of the glass was immersed in a growth solution in EtOH/H_2O (3:1 *v/v*) containing MBA (412 μM), $HAuCl_4$ (860 μM) and ascorbic acid (2 mM). After the addition of ascorbic acid, stirring was maintained for a few more seconds to mix all the components and then turned off. To stop growth at any point during the synthesis, the substrate was extracted from the solution, washed with EtOH to remove unbound MBA and dried under N_2.

Preparation of TEM grids: NWs were extracted into solution by washing the substrate with EtOH after growth, then soaking it in milli-Q H_2O and immersing in a sonicator bath for 15 min. Importantly, the sample should not be allowed to dry after washing. The NWs were then centrifuged and re-dispersed in milli-Q H_2O and several drops were casted on the grid and dried in air.

Detection in solution: Each sample was exposed to Ar^+ plasma cleaning (4 W, 10 mTorr of Ar inside the sputtering chamber) for 6 min. Cleaned samples were cut into stripes (~0.7 cm) and dipped in MG solutions with different concentrations for 1 h. For the successive detection of MG, 1-NAT and R6G, the cleaning/dipping steps were repeated three times.

Gas sensing: To ensure a closed environment during gas detection, the samples were fixed inside 25 mL plastic tubes containing drops of 1-NAT solutions in EtOH at different concentrations. Regarding the saturation curve, 10 samples were placed in 10 different tubes, all containing a 1-NAT drop (10^{-1} M) and extracted after selected times.

Acknowledgements

The authors acknowledge financial support from the European Research Council (ERC Advanced Grant) (267867-PLASMAQUO). We thank Chirstopher Tollan (CIC nanoGUNE) for assistance with SEM measurements and Elmira Farrokh Takin for help with nanowire growth.

Keywords: gold · nanowires · plasmonics · surface enhanced Raman scattering · ultradetection · molecular sensors

[1] M. Moskovits, *J. Raman Spectrosc.* **2005**, *36*, 485 – 496.
[2] M. Quinten, *Appl. Phys. B* **2001**, *73*, 245 – 255.
[3] J. M. McMahon, S. Li, L. K. Ausman, G. C. Schatz, *J. Phys. Chem. C* **2012**, *116*, 1627 – 1637.
[4] K. E. Shafer-Peltier, C. L. Haynes, M. R. Glucksberg, R. P. Van Duyne, *J. Am. Chem. Soc.* **2003**, *125*, 588 – 593.
[5] J. Kneipp, H. Kneipp, M. McLaughlin, D. Brown, K. Kneipp, *Nano Lett.* **2006**, *6*, 2225 – 2231.
[6] T. Vo-Dinh, F. Yan, M. B. Wabuyele, *J. Raman Spectrosc.* **2005**, *36*, 640 – 647.
[7] R. A. Alvarez-Puebla, E. R. Zubarev, N. A. Kotov, L. M. Liz-Marzán, *Nano Today* **2012**, *7*, 6 – 9.
[8] M. Sanles-Sobrido, L. Rodríguez-Lorenzo, S. Lorenzo-Abalde, Á. González-Fernández, M. A. Correa-Duarte, R. A. Alvarez-Puebla, L. M. Liz-Marzán, *Nanoscale* **2009**, *1*, 153 – 158.
[9] S. S. R. Dasary, A. K. Singh, D. Senapati, H. Yu, P. C. Ray, *J. Am. Chem. Soc.* **2009**, *131*, 13806 – 13812.
[10] M. Harz, P. Rösch, K.-D. Peschke, O. Ronneberger, H. Burkhardt, J. Popp, *Analyst* **2005**, *130*, 1543 – 1550.
[11] M. Leona, J. Stenger, E. Ferloni, *J. Raman Spectrosc.* **2006**, *37*, 981 – 992.
[12] K. L. Wustholz, C. L. Brosseau, F. Casadio, R. P. V. Duyne, *Phys. Chem. Chem. Phys.* **2009**, *11*, 7350 – 7359.
[13] H. Wang, C. S. Levin, N. J. Halas, *J. Am. Chem. Soc.* **2005**, *127*, 14992 – 14993.
[14] S. B. Chaney, S. Shanmukh, R. A. Dluhy, Y.-P. Zhao, *Appl. Phys. Lett.* **2005**, *87*, 031908.
[15] S. Gómez-Graña, J. Pérez-Juste, R. A. Alvarez-Puebla, A. Guerrero-Martínez, L. M. Liz-Marzán, *Adv. Opt. Mater.* **2013**, *1*, 477 – 481.
[16] E. Nalbant Esenturk, A. R. Hight Walker, *J. Raman Spectrosc.* **2009**, *40*, 86 – 91.
[17] G. Lu, C. Li, G. Shi, *Chem. Mater.* **2007**, *19*, 3433 – 3440.
[18] P. Xu, N. H. Mack, S.-H. Jeon, S. K. Doorn, X. Han, H.-L. Wang, *Langmuir* **2010**, *26*, 8882 – 8886.
[19] J. M. McLellan, A. Siekkinen, J. Chen, Y. Xia, *Chem. Phys. Lett.* **2006**, *427*, 122 – 126.
[20] R. A. Alvarez-Puebla, A. Agarwal, P. Manna, B. P. Khanal, P. Aldeanueva-Potel, E. Carbó-Argibay, N. Pazos-Pérez, L. Vigderman, E. R. Zubarev, N. A. Kotov, L. M. Liz-Marzán, *Proc. Natl. Acad. Sci. USA* **2011**, *108*, 8157 – 8161.
[21] Y. Zhu, H. Kuang, L. Xu, W. Ma, C. Peng, Y. Hua, L. Wang, C. Xu, *J. Mater. Chem.* **2012**, *22*, 2387 – 2391.
[22] Y. Zheng, T. Thai, P. Reineck, L. Qiu, Y. Guo, U. Bach, *Adv. Funct. Mater.* **2013**, *23*, 1519 – 1526.
[23] L. Gunnarsson, E. J. Bjerneld, H. Xu, S. Petronis, B. Kasemo, M. Käll, *Appl. Phys. Lett.* **2001**, *78*, 802 – 804.
[24] N. Félidj, J. Aubard, G. Lévi, J. R. Krenn, M. Salerno, G. Schider, B. Lamprecht, A. Leitner, F. R. Aussenegg, *Phys. Rev. B* **2002**, *65*, 075419.
[25] M. Kahl, E. Voges, S. Kostrewa, C. Viets, W. Hill, *Sens. Actuators B* **1998**, *51*, 285 – 291.
[26] Q. Min, M. J. L. Santos, E. M. Girotto, A. G. Brolo, R. Gordon, *J. Phys. Chem. C* **2008**, *112*, 15098 – 15101.
[27] A. Gopinath, S. V. Boriskina, W. R. Premasiri, L. Ziegler, B. M. Reinhard, L. Dal Negro, *Nano Lett.* **2009**, *9*, 3922 – 3929.
[28] F. S. Ou, M. Hu, I. Naumov, A. Kim, W. Wu, A. M. Bratkovsky, X. Li, R. S. Williams, Z. Li, *Nano Lett.* **2011**, *11*, 2538 – 2542.
[29] S. M. Wells, I. A. Merkulov, I. I. Kravchenko, N. V. Lavrik, M. J. Sepaniak, *ACS Nano* **2012**, *6*, 2948 – 2959.
[30] J. Yang, M. Palla, F. G. Bosco, T. Rindzevicius, T. S. Alstrøm, M. S. Schmidt, A. Boisen, J. Ju, Q. Lin, *ACS Nano* **2013**, *7*, 5350 – 5359.
[31] S. Srivastava, R. Sinha, D. Roy, *Aquat. Toxicol.* **2004**, *66*, 319 – 329.
[32] S. J. Culp, F. A. Beland, *Int. J. Toxicol.* **1996**, *15*, 219 – 238.
[33] A. Panandiker, C. Fernandes, T. K. Rao, K. V. Rao, *Cancer Lett.* **1993**, *74*, 31 – 36.

[34] K. V. K. Rao, *Toxicol. Lett.* **1995**, *81*, 107 – 113.
[35] J. He, Y. Wang, Y. Feng, X. Qi, Z. Zeng, Q. Liu, W. S. Teo, C. L. Gan, H. Zhang, H. Chen, *ACS Nano* **2013**, *7*, 2733 – 2740.
[36] A. M. Funston, C. Novo, T. J. Davis, P. Mulvaney, *Nano Lett.* **2009**, *9*, 1651 – 1658.
[37] M. I. Dar, S. Sampath, S. A. Shivashankar, *J. Mater. Chem.* **2012**, *22*, 22418 – 22423.
[38] P. L. Stiles, J. A. Dieringer, N. C. Shah, R. P. Van Duyne, *Annu. Rev. Anal. Chem.* **2008**, *1*, 601 – 626.
[39] S. Lee, J. Choi, L. Chen, B. Park, J. B. Kyong, G. H. Seong, J. Choo, Y. Lee, K.-H. Shin, E. K. Lee, S. W. Joo, K.-H. Lee, *Anal. Chim. Acta* **2007**, *590*, 139 – 144.
[40] H. B. Lueck, D. C. Daniel, J. L. McHale, *J. Raman Spectrosc.* **1993**, *24*, 363 – 370.
[41] R. A. Alvarez-Puebla, D. S. Dos Santos, R. F. Aroca, *Analyst* **2004**, *129*, 1251 – 1256.
[42] M. Baia, L. Baia, S. Astilean, *Chem. Phys. Lett.* **2005**, *404*, 3 – 8.

Received: April 10, 2014
Published online on July 9, 2014